



Exploring the influence of friction in the puncture mechanics of soft solids

Matteo Montanari · Andrea Spagnoli

Received: 19 September 2023 / Accepted: 12 February 2024
© The Author(s) 2024

Abstract Friction is an ever-present force in our lives, affecting the interaction between objects in numerous ways. The common hypothesis of frictionless contact between a foreign rigid object (needle) and a target material during puncturing leads to a constant penetration force. However, experimental observations reveal a linear increase in penetration force as the needle tip delves deeper. This force increment arises from the interplay of friction and adhesion at needle-solid interface. The present work provides an insight into the measure of friction and adhesion quasi-static characteristics at the needle-solid interface through puncture experiments. To this end, an axisymmetric hyperelastic model is presented to describe the expansion of a cavity under the contact pressure of the penetrating needle. In addition, the competing mechanisms of cavity expansion and mode I cracking during needle penetration in a soft solid are discussed.

Keywords Puncturing · Soft material · Adhesion · Friction

M. Montanari · A. Spagnoli (✉)
Department of Engineering and Architecture, University of Parma, Parco Area delle Scienze 181/A, 43124 Parma, Italy
e-mail: andrea.spagnoli@unipr.it

M. Montanari
e-mail: matteo.montanari@unipr.it

1 Introduction

For decades, the mechanics of deep penetration has been extensively studied due to its wide-ranging applications in engineering and medicine. The focus lies in investigating the behaviour of a foreign object, as it deeply penetrates a soft target material. Penetration inevitably involves laceration of the material and/or expansion of existing flaws in the material itself. Typically, the penetrating object is a rigid tool, but also flexible needles are explored in the literature (e.g. see [1–8]). The mechanics of puncturing is relevant in several applications in medical procedures, both manual and automated, such as injections [9], blood testing [10], biopsies [11], and design of advanced surgical instruments [12]. Additionally, deep penetration plays a crucial role in essential natural processes within living organisms where tissue penetration is vital. To gain a better understanding of the mechanical aspects of puncture with respect to material properties, extensive experimentation, numerical and theoretical analyses have been conducted, both on solid blocks of materials [13–27] and on thin membranes [28–38].

However, one aspect that has received relatively little attention is the role of friction in this process, and a comprehensive exploration of this phenomenon is lacking in the current scientific literature. Most of the existing theoretical models rely on the assumption of frictionless contact, resulting in a penetration force that remains independent of the needle's depth within

the material. This contradicts experimental findings, which indicate a linear increase in force with depth during puncture experiments. The force increment can be attributed to the effects of friction and adhesion between the needle and the solid, and it should be accurately quantified to provide a detailed description of the phenomenon. For this purpose, through numerical simulations, Fregonese and Bacca [39] established a correlation between the force-displacement slope and various material properties and geometrical features such as rigidity, toughness, radius of the penetrator, and interfacial strength.

In this paper, an experimental campaign is carried out on the quasi-static penetration of a rigid needle into a soft solid containing a coaxial cylindrical cavity. Depending on the misfit between needle diameter and cavity dimension, and considering the axisymmetric hyperelastic solution of an expanding circular hole, the parameters describing the interface bond between needle and material can experimentally be quantified. Such parameters are then used to interpret the experimental load–displacement curves of needle penetration into a bulk solid, involving the mechanism of laceration of the material. To this end, a theoretical model describing the needle penetration due to mode I cracking is presented.

2 Energy balance during the deep penetration of a needle

The mechanics of an object piercing a target solid can be characterised by two different stages: an initial stage of *indentation* and a subsequent stage of *penetration*. In the former, the tip of the indenter is in contact with the target bulk solid, which accumulates strain energy while the indentation progresses. The indentation stage terminates when an energetically favourable mechanism of laceration takes place in the target solid [22]. According to Shergold and Fleck [40], for soft materials either mode-II crack ring or mode-I planar cracks develop for flat-bottomed punch and sharp-tipped punch, respectively. The latter mechanism features the development of a crack linearly increasing its depth with the penetration depth of the indenter.

In the present paper, a rigid sharp-tipped punch (needle) of radius R is assumed to penetrate a large soft solid along a direction normal to the surface of

the solid. The puncturing process which takes place in the material can be described using an energy-based formulation. Neglecting inelastic phenomena in the bulk of the material, the increment of external work generated by the puncturing force is consumed by the elastic strain energy, the work of fracture and the frictional dissipation. The general incremental form of the energy balance is

$$dU_{\text{ext}} = dU_s + dU_G + dU_f, \quad (1)$$

where dU_{ext} is the external work input, dU_s is the strain energy variation in the solid, dU_G is the energy spent to advance the crack, and dU_f is the energy dissipated due to friction at the needle–solid interface. A force F is exerted on the needle in order to penetrate a small amount dD , so that $dU_{\text{ext}} = FdD$.

3 Mechanism of needle penetration by mode I cracking

3.1 Linear elastic fracture mechanics formulation

This section briefly summarises a theoretical model (details of the solution to this problem are provided in Terzano et al. [41] and Spagnoli et al. [42]) that explores the steady-state penetration of a needle employing the principles of linear elastic fracture mechanics (LEFM). The model considers the plane strain problem related to a cross section of the target solid normal to the penetration direction. Accordingly, the mode I crack, featuring a crack plane of dimensions $2a \times D$, is opened by the action of the needle (Fig. 1). The target solid is constituted by a bulk material, i.e. containing no flaws or cavities ($b = 0$ according to the nomenclature of Fig. 3 below).

Such an action imposes prescribed opening displacements to the crack faces where the needle is in contact with the target material. The resulting stress intensity factor (SIF), K , is illustrated in Fig. 2 as a function of the normalised needle radius R/a . Also, the position of the point of separation at the needle–solid interface a_1 is shown against the R/a ratio. The SIF is normalised with respect to K_R , namely the stress intensity factor related to the needle filling the entire crack ($R/a = 1$). This is defined as

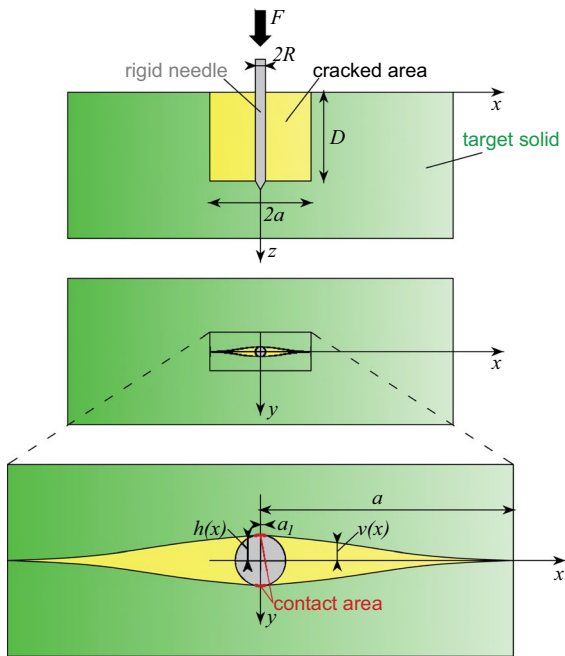


Fig. 1 Sketch depicting the mode-I crack mechanism during the continuous penetration of a rigid circular needle into a target bulk solid. The enlarged view reveals the crack’s shape and its contact area with the needle. The dimensions provided in the drawings refer to the initial, undeformed state; such dimensions are not to scale and are shown in this form for the sake of graphical clarity

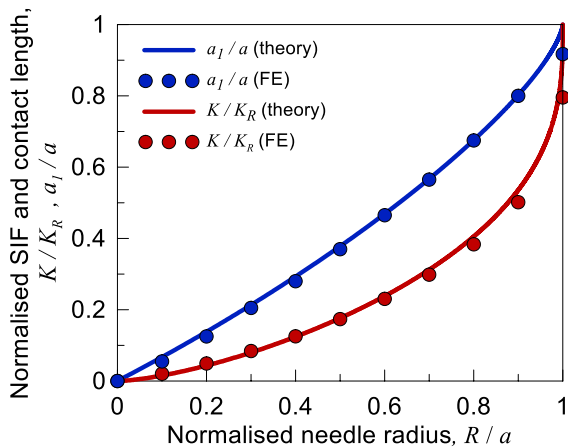


Fig. 2 LEFM model of puncturing: normalised SIF and contact length against normalised relative radius of the penetrating needle

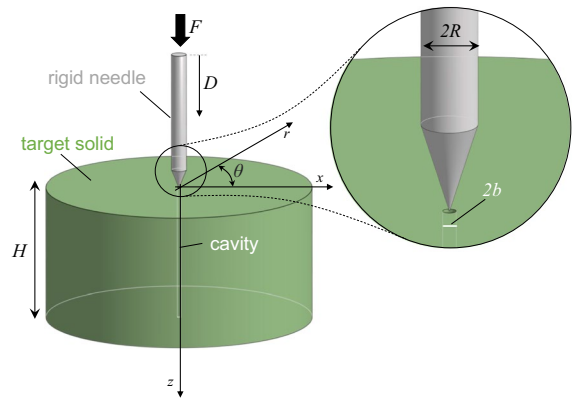


Fig. 3 Sketch of the puncturing mechanism for evaluating the frictional characteristics during the penetration of a rigid circular needle into a target solid containing a cylindrical cavity of radius b (with $R \geq b$)

$$K_R = \frac{E^*}{2} \sqrt{\pi R}. \tag{2}$$

where $E^* = E/(1 - \nu^2)$. Figure 2 can be employed to determine the critical condition of crack propagation, for a given radius of the needle and fracture toughness K_c of the target material (based on Irwin’s relation of LEFM $K_c = \sqrt{E^*G_c}$, where $G_c =$ fracture energy). According to the LEFM model, the planar crack of semi-length a forms so that $K = K_c$ at the crack tips. The critical value of the relative radius R/a as well as the critical value of the contact relative semi-length a_1/a are therefore obtained from Fig. 2 by posing $K = K_c$.

3.2 Contact pressure and frictional characteristics

When the needle penetrates for a depth D , strain energy accumulates in the target material due to its deformation induced by the contact pressure at the needle-solid interface. As a first estimation, we assume a uniform contact pressure equal to $q = E^*/2$ acting on a contact length $2a_1$. Such a contact pressure corresponds to the traction applied to the crack face which produces a maximum crack opening displacement equal to the needle radius R [43]. Alternatively, the contact pressure can be calculated by considering an Hertzian contact between the needle and the solid. The assumption of uniform contact pressure is appropriate when $a_1/a \rightarrow 1$ [41, 42].

In the presence of friction and adhesion, by considering the actual surface of the needle-solid interface in the deformed configuration, the work done by the frictional forces required to push the needle by a depth dD is

$$dU_f = (c + \xi q)2\pi a_1 D dD = (c + \xi q) \left(\frac{a_1}{a}\right) \left(\frac{a}{R}\right) 2\pi R D dD, \tag{3}$$

where c is the adhesion shear stress, ξ is the Coulomb friction coefficient and q is the contact pressure between the solid and the lateral surface of the needle. In Eq. 3, the normalised lengths a_1/a and R/a are deliberately introduced to highlight the dependence of dU_f on the material toughness (see Fig. 2). The adhesion contribution c accounts for the sliding resistance in the absence of a contact pressure ($q = 0$). The derivative of U_f in Eq. 3 with respect to D yields the frictional force

$$F_f = \frac{dU_f}{dD} = (c + \xi q) \left(\frac{a_1}{a}\right) \left(\frac{a}{R}\right) 2\pi R D \tag{4}$$

Equation 4 shows that the penetration force increases linearly with D , as it will be observed in experiments reported below. Hence, with the assumption of a constant contact pressure between the needle and the target material, it is possible to obtain the expression of the slope of the force-displacement curve (the other contributions related to strain energy and fracture energy are independent on D)

$$\frac{dF}{dD} = \pi \left(\frac{a_1}{a}\right) \left(\frac{a}{R}\right) R(2c + \xi E^*). \tag{5}$$

4 Mechanism of needle penetration by cavity expansion

In order to investigate the frictional interaction between the needle and the solid during the puncturing process, we decide to introduce *a priori* a cylindrical cavity of dimensions $(2b \times H)$ into the target solid (Fig. 3).

This approach enables us to evaluate the adhesion shear stress by employing a needle with the same radius as that of the cavity ($R = b$), while larger needles ($R > b$) are utilised to estimate the Coulomb friction coefficient. By taking $R = b$, the first two

components of the right hand side of Eq. 1 disappear and the external work is only balanced by the frictional contribution, therefore

$$dU_{\text{ext}} = dU_f \tag{6}$$

In the case of $R > b$, the incremental energy balance experiences the additional contribution of the strain energy, that is

$$dU_{\text{ext}} = dU_s + dU_f \tag{7}$$

where dU_s is independent on the penetration depth D as demonstrated in the next section.

The frictional energy dU_f takes the following form

$$dU_f = (c + \xi q)2\pi R D dD, \tag{8}$$

where the contact pressure q is given by the radial Cauchy stress derived in the next section.

4.1 Hyperelastic model for cavity expansion

In this section, we determine the stress and strain field in an infinite solid containing a circular cylindrical cavity enlarged from an initial radius b to a final radius R . We consider a slice of an hyperelastic large solid undergoing a perforation with a cylindrical needle. The slice is taken normal to the penetration direction of the needle, so that we can study a large plate of unit thickness under plane strain condition containing a cylindrical hole, expanded by the rigid circular cross section of the needle (see Fig. 4).

The problem is treated as an axisymmetric one so that the plate has an external radius $R_e \rightarrow \infty$. A cylindrical coordinate system $r\theta z$ is adopted in the deformed configuration so that $R \leq r$. The radial coordinate in the reference configuration is s , with $b \leq s$. Note that $(R - b)$ is the imposed radial displacement on the internal cavity inducing its expansion.

Assuming isochoric deformations under plane strain condition of the material, the principal stretches are ($J = \lambda_r \lambda_\theta \lambda_z = 1$)

$$\lambda_r = \frac{s}{r}, \quad \lambda_\theta = \lambda_r^{-1} = \frac{r}{s}, \quad \lambda_z = 1 \tag{9}$$

Note that λ_r is the independent stretch during the axisymmetric deformation.

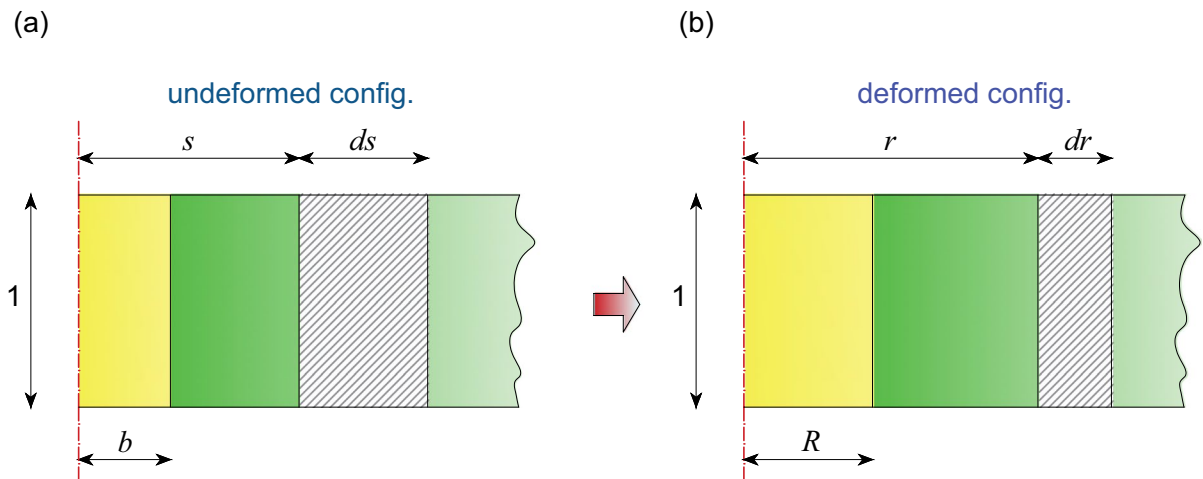


Fig. 4 Deformation of a cylindrical annulus of the solid of unit height from a radius s to a radius r , due to the expansion of a cavity from a radius b to a radius R : **a** undeformed configuration, **b** deformed configuration

Let us take an Ogden potential [44] with $\alpha = 2$ (Neo-Hookean material)

$$\Psi = \frac{\mu}{2}(\lambda_r^2 + \lambda_\theta^2 + \lambda_z^2 - 3) - p(J - 1) \tag{10}$$

where p is the hydrostatic pressure. The Neo-Hookean model is widely used to characterise the nonlinear stress–strain behaviour of materials undergoing large deformations. This model relies solely on a single constant, the initial shear modulus μ , being incompressibility assumed.

By derivation we obtain the principal Cauchy stresses ($\sigma_a = \sigma_r, \sigma_\theta, \sigma_z$) from

$$\sigma_a = J^{-1} \lambda_a \frac{\partial \Psi}{\partial \lambda_a} = \mu \lambda_a^2 - p \tag{11}$$

that are

$$\sigma_r = \mu \lambda^2 - p, \quad \sigma_\theta = \mu \lambda^{-2} - p, \quad \sigma_z = \mu - p \tag{12}$$

where $\lambda = \lambda_r$.

Now, by exploiting the isochoric condition $r^2 - R^2 = s^2 - b^2$, one can express the radial stretch as

$$\lambda = \sqrt{\frac{b^2}{r^2} - \frac{R^2}{r^2} + 1} \tag{13}$$

Then the equilibrium in the deformed configuration of a half elementary annulus of internal radius r and of thickness dr yields

$$r \frac{d\sigma_r}{dr} + \sigma_r = \sigma_\theta \tag{14}$$

By plugging into (14) the expressions of the principal stresses (12), since the first derivative of the function $\lambda(r)$ is

$$\frac{d\lambda}{dr} = \frac{R^2 - b^2}{r^2 \sqrt{b^2 + r^2 - R^2}}, \tag{15}$$

we obtain the following equation of the hydrostatic pressure p

$$\begin{aligned} \frac{dp}{dr} = & 2\mu \frac{R^2 - b^2}{r^2 \sqrt{b^2 + r^2 - R^2}} \sqrt{\frac{b^2}{r^2} - \frac{R^2}{r^2} + 1} + \\ & + \mu \left(\frac{r}{R^2 - b^2 - r^2} - \frac{R^2}{r^3} + \frac{b^2}{r^3} + \frac{1}{r} \right) \end{aligned} \tag{16}$$

By integrating Eq. (16) we finally get

$$\begin{aligned} \frac{p(r)}{\mu} = & \frac{(b^2 - R^2)}{2r^2} + \\ & + \frac{1}{2} (\log(r^2) - \log(b^2 + r^2 - R^2)) + C \end{aligned} \tag{17}$$

where the integration constant C can be obtained by imposing the equilibrium boundary condition of $\sigma_r = 0$ at $r = R_e$. A graphical representation of the radial stress σ_r (see Eqs. 12 and 17) is given in Fig. 5, for different needle diameters. Figure 5 offers a view of the radial true stress as a function of the radial

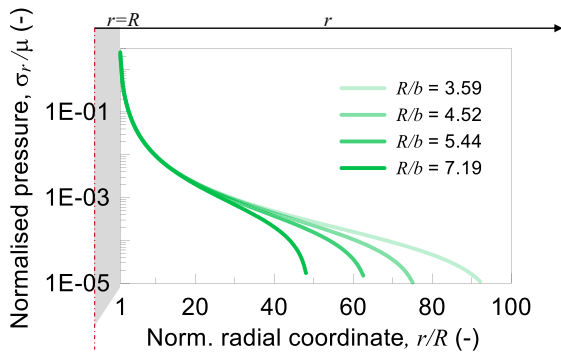


Fig. 5 Normalised radial stress σ_r against normalised radial coordinate, for increasing needle radius R with respect to the cavity radius b

coordinate in the deformed configuration, for different values of R/b ratio. Such plot could be useful to have an insight of the stress state in the target material, as well as of the contact pressure at the needle-solid interface.

The total strain energy stored in the solid slice of unit thickness (with $R_e \rightarrow \infty$) due to a cavity expansion from radius b to R is obtained by

$$\frac{dU_s}{dD} = 2\pi \int_R^\infty \Psi r dr \tag{18}$$

which results in

$$\frac{dU_s}{dD} = \pi\mu R^2 \left(\frac{b^2}{R^2} - 1 \right) \log\left(\frac{b}{R}\right) \tag{19}$$

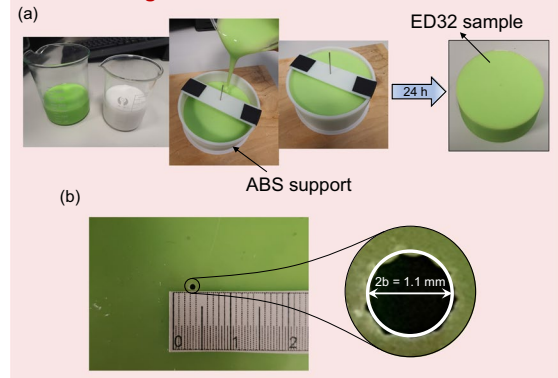
Note that the quantity in Eq. 19 corresponds to the constant force F_e required to expand the cavity during needle penetration.

5 Experiments and discussion

In order to verify the theoretical findings presented in the previous sections, a series of experiments have been carried out.

Cylindrical samples have been manufactured with a commercial silicone, Elite Double 32 (ED32) by Zhermack Dental. This silicone is a Polyvinyl Siloxane (PVS) elastomer, widely employed for model duplication in the dentistry field. An FDM 3D printed cylindrical specimen made of Acrylonitrile Butadiene

Manufacturing



Experiments

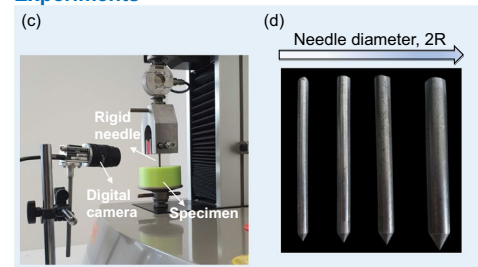


Fig. 6 Manufacturing procedure of the silicone specimens (a), dimension of the cavity (b), experimental setup (c), view of the needles used in the experiments (d)

Styrene (ABS) has been used as a mould for the silicone.

The preparation protocol of a representative silicone sample is summarised in Fig. 6a. The mechanical parameters of such a silicone are taken from Montanari et al. [14]. In particular, assuming the silicone to be incompressible, $E^* = 4\mu = 1.215$ MPa and $G_c = 1.162$ N/mm. All the puncturing experiments have been performed on a cylindrical sample with radius R_e equal to 45 mm and height H equal to 45 mm. The specimens contain a central cylindrical cavity with radius equal to $b = 0.55$ mm and height H , see Fig. 3. A sharp-tipped steel punch (tip opening angle α equal to 30 deg) with circular cross-section having different diameters ($2R = 3.95, 4.97, 5.98, 7.91$ mm) is inserted under displacement-control into the target material at a constant speed of 1 mm/min (Fig. 6d). All the mechanical tests are performed by using a universal testing machine Galdabini Quasar 2.5, equipped with a 3 kN load cell, with computer control and data acquiring system, at a room temperature

of 20 °C, 24 h after the preparation of the specimens. Pictures during the experiments are taken by means of a Basler acA5472-17uc USB 3.0 camera (Fig. 6c).

Results of the puncturing experiments related to specimens containing a cavity are illustrated in Fig. 7a. Here, the force-displacement curves obtained during the puncturing tests are shown separately for each needle diameter. From the analysis of the results, it turns out that such curves can be divided in two different regions: the first one governed by the hyperelastic deformation of the cavity expanding in the solid while the second one, corresponding to the linear region, in which friction between the needle and the solid is the only mechanism involved. The cavity expansion force F_e is identified as the force at the onset of the linear behaviour. Figure 7b shows pictures of a puncturing test

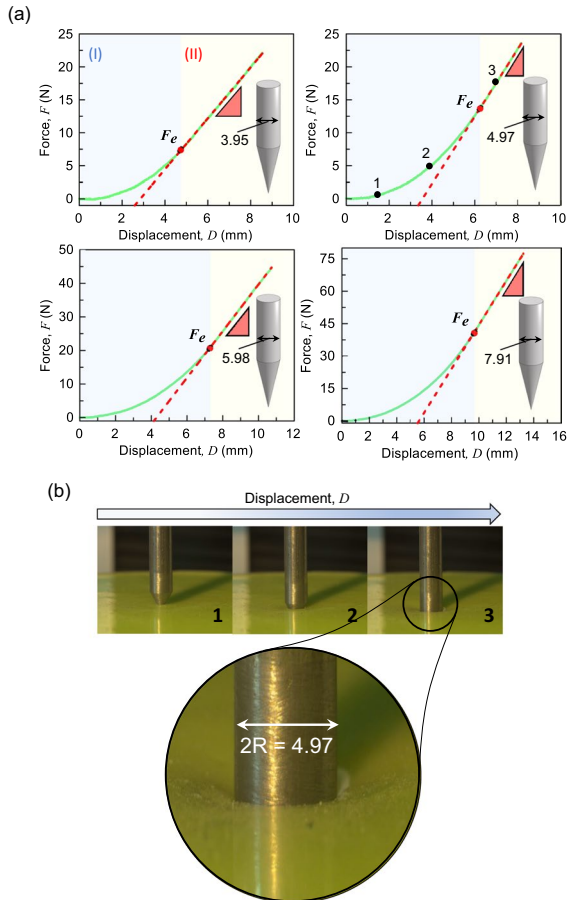


Fig. 7 Force-displacement curves resulting from the puncturing experiments on samples with a cylindrical cavity, for different needle diameters (a) and pictures of a puncturing test at different needle depths (see chart on top right in a) (b)

using a needle with diameter $2R = 4.97$ mm, at different applied displacements.

Moreover, Fig. 8 shows the results of puncturing experiments, taken from Montanari et al. [14], on bulk silicone samples (with no cavity, $b = 0$) using different diameters ($2R = 1.28, 1.50, 2.15, 2.72$ mm). From these curves it is possible to define the penetration force F_p as the point at which steady-state penetration begins, occurring after material rupture and subsequent relaxation.

In order to evaluate both friction and adhesion between the needle and the solid, we performed an experiment on the sample with the cavity but employing a needle with diameter $2R$ equal to 1.1 mm (the same as the cavity $2b$). The resulting force-displacement curve is presented in 9a. From the slope of the curve divided by $2\pi R$ (see Eq. 8 with $q = 0$ and its second order derivative with respect to D), it is possible to estimate $c = 40$ kPa.

On the other hand, from the slopes of the linear region of the experimental curves presented in Fig. 7a, it is possible to estimate the friction coefficient ξ . In particular, by inverting the second derivative with respect to D of U_f in Eq. 8,

$$\xi = \frac{1}{q} \left(\frac{dF/dD}{2\pi R} - c \right) \tag{20}$$

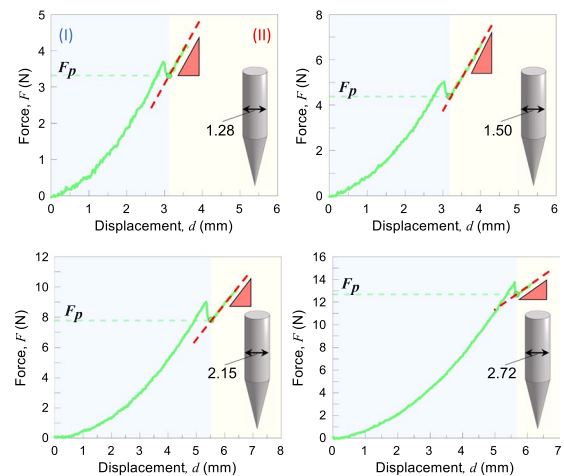


Fig. 8 Force-displacement curves resulting from the puncturing experiments on bulk specimens ($b = 0$), for different needle diameters. Load–displacement slope in the post-fracture region is highlighted by a dashed red line

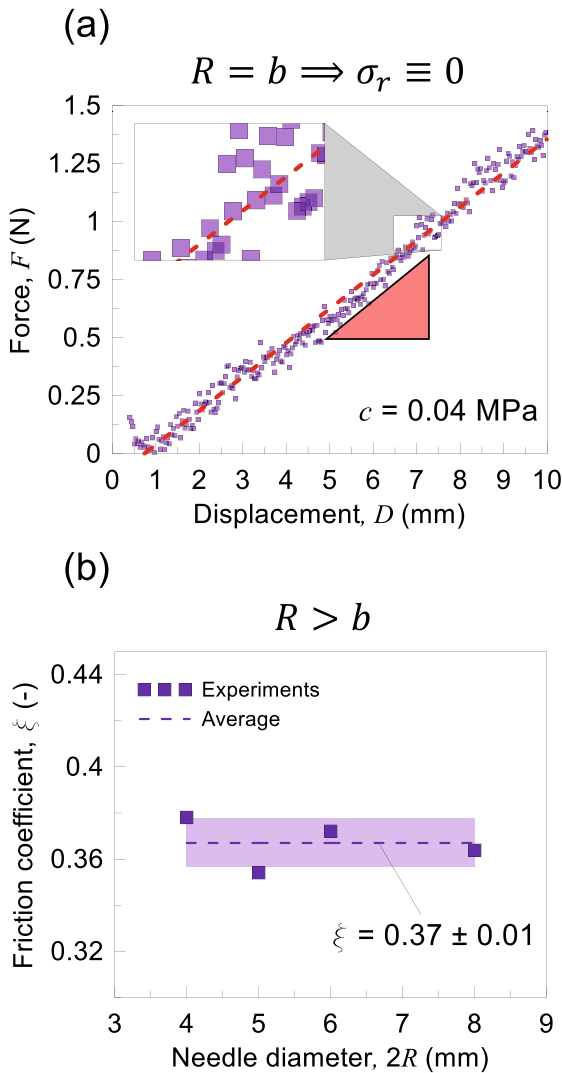


Fig. 9 Force-displacement curve and linear fitting (dashed red line) resulting from the *friction test* (cavity with $b = R$) (a), friction coefficients (experimental data, average and standard deviation) evaluated for the different needle diameters (cavity with $R > b$) (b)

where $q = \sigma_r(r = R)$ (see Eqs. 12 and 17), it is possible to estimate an average Coulomb friction coefficient equal to $\xi = 0.37$ (see Fig. 9b).

Figure 10 shows the experimentally obtained hole expansion forces F_e in the voided specimens with cavity ($b < R$) and force slope dF/dD in the bulk specimens without cavity ($b = 0$), respectively, for the various needle diameters. In addition, the theoretical results are also reported, where the expansion force is calculated according to Eq. 19 and the force

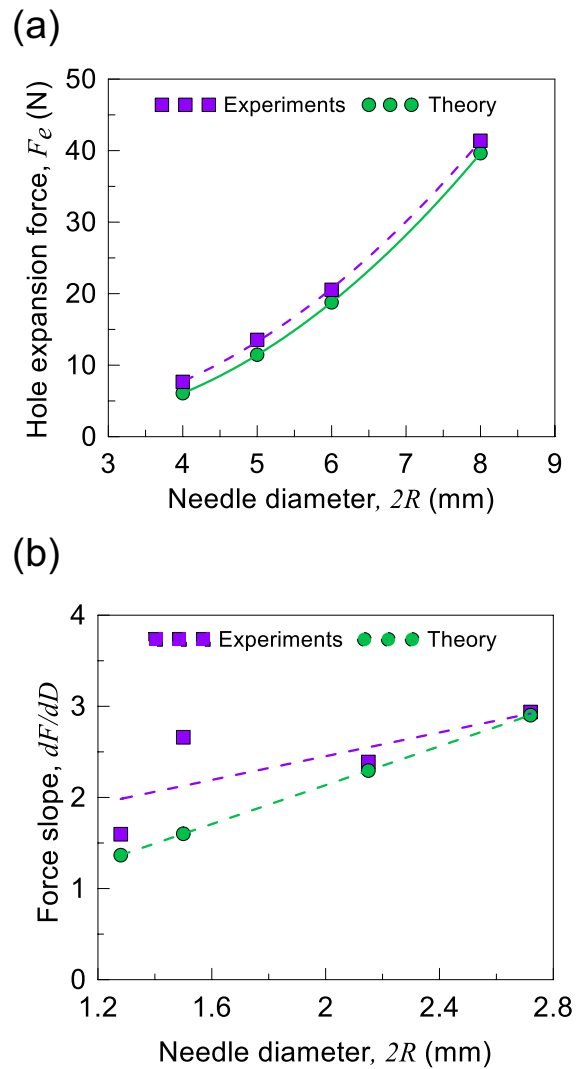


Fig. 10 Theoretical and experimental results of the cavity expansion force F_e in the specimens with cavity ($b < R$) (a) and force slope dF/dD in the specimens without cavity ($b = 0$) (b), against the needle diameter

slope according to Eq. 5 with $a_1/a \approx 1$ and $R/a \approx 1$ for the material under consideration. The results turn out to be quite satisfactory, since an overall average 15% error is obtained.

6 Conclusion

This work delves into the interplay of friction and adhesion at the interface between the needle and solid material during quasi-static puncture experiments.

In particular, we introduce a novel experimental approach for assessing the frictional characteristics of a rigid needle as it penetrates a soft material.

Several experiments are carried out by inserting a rigid sharp-tipped punch with circular cross section of radius R in silicone specimens containing an initial cylindrical cavity of radius $b \leq R$. The results in terms of penetration force-displacement curves, together with the theoretical findings related to the hole expansion in an hyperelastic solid, are employed to determine the relevant friction parameters at the needle-solid interface: the adhesive shear stress c and the Coulomb friction coefficient ξ . Such parameters allow the estimation of the load-displacement slope dF/dD in the steady state needle penetration into a bulk solid. Furthermore, the investigation explores the mechanism of cavity expansion, offering initial insights into the behaviour of flawed soft solids during needle penetration. The comparison between the theoretical and experimental outcomes, in terms of force slopes dF/dD and cavity expansion forces F_e , is quite good, as it yields an overall average error of about 15%. The competing mechanism of needle penetration due to mode I cracking is also discussed on the basis of a simple theoretical model based on linear elastic fracture mechanics.

This work might serve as a valuable tool for predicting the needle-tissue mechanical interaction in biomedical applications, such as robot-assisted surgical procedures.

Author contributions M.M.: Methodology, Investigation, Visualisation, Writing - Original Draft. A.S.: Conceptualisation, Writing - Review and Editing, Supervision.

Funding Open access funding provided by Università degli Studi di Parma within the CRUI-CARE Agreement.

Declarations

Competing interest The authors declare that they have no known competing financial interests or personal relationships that could have appeared to influence the work reported in this paper.

Open Access This article is licensed under a Creative Commons Attribution 4.0 International License, which permits use, sharing, adaptation, distribution and reproduction in any medium or format, as long as you give appropriate credit to the original author(s) and the source, provide a link to the Creative Commons licence, and indicate if changes were made. The images or other third party material in this article are included

in the article's Creative Commons licence, unless indicated otherwise in a credit line to the material. If material is not included in the article's Creative Commons licence and your intended use is not permitted by statutory regulation or exceeds the permitted use, you will need to obtain permission directly from the copyright holder. To view a copy of this licence, visit <http://creativecommons.org/licenses/by/4.0/>.

References

- Goksel O, Dehghan E, Salcudean SE (2009) Modeling and simulation of flexible needles. *Med Eng Phys* 31:1069–1078
- Misra S, Reed K, Schafer B, Ramesh K, Okamura A (2010) Mechanics of flexible needles robotically steered through soft tissue. *Int J Robot Res* 29:1640–1660
- Lee H, Kim J (2014) Estimation of flexible needle deflection in layered soft tissues with different elastic moduli. *Med Biol Eng Comput* 52:729–740
- Terzano M, Dini D, Rodriguez y Baena F, Spagnoli A, Oldfield M (2020) An adaptive finite element model for steerable needles. *Biomech Model Mechanobiol* 19:1809–1825
- Liu W, Yang Z, Fang P, Jiang S (2020) Deflection simulation for a needle adjusted by the insertion orientation angle and axial rotation during insertion in the muscle-contained double-layered tissue. *Med Biol Eng Comput* 58:2291–2304
- Cai C, Sun C, Han Y, Zhang Q (2020) Clinical flexible needle puncture path planning based on particle swarm optimization. *Comput Methods Programs Biomed* 193:105511
- Feng S, Wang S, Jiang W, Gao X (2023) Planning of medical flexible needle motion in effective area of clinical puncture. *Sensors* 23:671
- Martopoulou A, Hill TL, Persad R, Bolomytis S, Tzemanaki A (2023) Modelling and real-time dynamic simulation of flexible needles for prostate biopsy and brachytherapy. *Math Comput Model Dyn Syst* 29:1–40
- DiMaio S, Salcudean S (2003) Needle insertion modeling and simulation. *IEEE Trans Robot Autom* 19:864–875
- Torossian K, Ottenio M, Brulez A-C, Lafon Y, Benayoun S (2019) Biomechanics of the medical gesture for a peripheral venous catheter insertion. *Comput Methods Biomech Biomed Eng* 22:S294–S295
- Moore JZ, McLaughlin PW, Shih AJ (2012) Novel needle cutting edge geometry for end-cut biopsy. *Med Phys* 39:99–108
- Nelson CA (2013) Material selection indices for design of surgical instruments with long tubular shafts. *J Med Eng Technol* 37:102–108
- Triki E, Gauvin C (2019) Stress state analysis and tensile-shear fracture criterion in combined puncture and cutting of soft materials. *Eng Fail Anal* 106:104140
- Montanari M, Brighenti R, Terzano M, Spagnoli A (2023) Puncturing of soft tissues: experimental and fracture mechanics-based study. *Soft Matter* 19:3629–3639

15. Gzaïel M, Triki E, Barkaoui A (2019) Finite element modeling of the puncture-cutting response of soft material by a pointed blade. *Mech Mater* 136:103082
16. Bao YD, Qu SQ, Qi DB, Wei W (2022) Investigation on puncture mechanical performance of tracheal tissue. *J Mech Behav Biomed Mater* 125:104958
17. Fakhouri S, Hutchens SB, Crosby AJ (2015) Puncture mechanics of soft solids. *Soft Matter* 11:4723–4730
18. Das S, Laha S, Ghatak A (2014) A co-operative effect of closely spaced intruding objects puncturing into a soft solid. *Soft Matter* 10:6059
19. Al-Safadi S, Hutapea P (2023) A study on modeling the deflection of surgical needle during insertion into multi-layer tissues. *J Mech Behav Biomed Mater* 146:106071
20. Jiang S, Li P, Yu Y, Liu J, Yang Z (2014) Experimental study of needle-tissue interaction forces: effect of needle geometries, insertion methods and tissue characteristics. *J Biomech* 47:3344–3353
21. Kundan KK, Laha S, Ghatak A (2019) Vibration assisted puncturing of a soft brittle solid. *Extreme Mech Lett* 26:26–34
22. Fregonese S, Bacca M (2021) Piercing soft solids: a mechanical theory for needle insertion. *J Mech Phys Solids* 154:104497
23. Fregonese S, Tong Z, Wang S, Bacca M (2023) Theoretical puncture mechanics of soft compressible solids. *J Appl Mech* 90:111003
24. Rattan S, Crosby AJ (2019) Effect of polymer volume fraction on fracture initiation in soft gels at small length scales. *ACS Macro Lett* 8:492–498
25. Rattan S, Crosby AJ (2018) Effect of far-field compliance on local failure dynamics of soft solids. *Extreme Mech Lett* 24:14–20
26. Gidde STR, Islam S, Kim A, Hutapea P (2023) Experimental study of mosquito-inspired needle to minimize insertion force and tissue deformation. *Proc Inst Mech Eng* 237:113–123
27. Patel KI, Zhu L, Ren F, Hutapea P (2021) Effect of composite coating on insertion mechanics of needle structure in soft materials. *Med Eng Phys* 95:104–110
28. Mohammadi H, Ebrahimian A, Maftoon N (2023) Cutting characteristics of viscoelastic membranes under hypodermic needle insertion. *Int J Mech Sci* 262:108717
29. Jiang Z, Liu J, Li Y, Kang G (2022) Indentation and puncture of double-network tough hydrogel membranes. *Polym Test* 116:107782
30. Liu J et al (2022) Indentation of elastomeric membranes by sphere-tipped indenters: snap-through instability, shrinkage, and puncture. *J Mech Phys Solids* 167:104973
31. Triki E, Gauvin C (2019) Analytical and experimental investigation of puncture-cut resistance of soft membranes. *Mech Soft Mater* 1:6
32. Aernouts J, Aerts JR, Dirckx JJ (2012) Mechanical properties of human tympanic membrane in the quasi-static regime from in situ point indentation measurements. *Hear Res* 290:45–54
33. Liu J et al (2018) Puncture mechanics of soft elastomeric membrane with large deformation by rigid cylindrical indenter. *J Mech Phys Solids* 112:458–471
34. Deris AH, Nadler B (2015) Modeling the indentation and puncturing of inflated elastic membranes by rigid indenters. *Int J Non-Linear Mech* 69:29–36
35. Saavedra VO, Fernandes TFD, Milhiet P-E, Costa L (2020) Compression, rupture, and puncture of model membranes at the molecular scale. *Langmuir* 36:5709–5716
36. Triki E (2016) Combined puncture/cutting of elastomer membranes by pointed blades: an alternative approach of fracture energy. *Mech Mater* 97:19–25
37. Triki E, Nguyen-Tri P, Gauvin C, Azaiez M, Vu-Khanh T (2015) Combined puncture/cutting of elastomer membranes by pointed blades: characterization of mechanisms. *J Appl Polym Sci* 132:42150
38. Saberi E, Najari SS, Abdollahi SB, Soltanzadeh Z (2017) A hyperelastic approach for finite element modelling puncture resistance of needle punched nonwoven geotextiles. *Fibers Polym* 18:1623–1628
39. Fregonese S, Bacca M (2022) How friction and adhesion affect the mechanics of deep penetration in soft solids. *Soft Matter* 18:6882–6887
40. Shergold OA, Fleck NA (2004) Mechanisms of deep penetration of soft solids, with application to the injection and wounding of skin. *Proc R Soc A Math Phys Eng Sci* 460:3037–3058
41. Terzano M, Spagnoli A, Stähle P (2018) A fracture mechanics model to study indentation cutting. *Fatigue Fract Eng Mater Struct* 41:821–830
42. Spagnoli A, Terzano M, Brighenti R, Artoni F, Stähle P (2018) The fracture mechanics in cutting: a comparative study on hard and soft polymeric materials. *Int J Mech Sci* 148:554–564
43. Terzano M, Spagnoli A, Stähle P (2018) A fracture mechanics model to study indentation cutting. *Fatigue Fract Eng Mater Struct* 41:821–830
44. Ogden RW (1972) Large deformation isotropic elasticity: on the correlation of theory and experiment for compressible rubberlike solids. *Proc R Soc Lond A Math Phys Sci* 328:567–583

Publisher's Note Springer Nature remains neutral with regard to jurisdictional claims in published maps and institutional affiliations.